Physica D 469 (2024) 134322

Contents lists available at ScienceDirect

Physica D

journal homepage: www.elsevier.com/locate/physd

Dynamics of liquid bridges between patterned surfaces

Margarida S. Rodrigues [a], Rodrigo C.V. Coelho [a,b], Paulo I.C. Teixeira [a,c,*]

[a] Centro de Física Teórica e Computacional, Faculdade de Ciências, Universidade de Lisboa, P-1749-016 Lisboa, Portugal
[b] Departamento de Física, Faculdade de Ciências, Universidade de Lisboa, P-1749-016 Lisboa, Portugal
[c] ISEL – Instituto Superior de Engenharia de Lisboa, Instituto Politécnico de Lisboa, Rua Conselheiro Emídio Navarro 1, 1959-007 Lisboa, Portugal

ARTICLE INFO

Communicated by Dmitry Pelinovsky

Keywords:
Liquid bridge
Binary fluids
Lattice Boltzmann method
Wetting
Fluid dynamics

ABSTRACT

We have simulated the motion of a single vertical, two-dimensional liquid bridge spanning the gap between two flat, horizontal solid substrates consisting of alternating hydrophilic and hydrophobic stripes, using a multicomponent pseudopotential lattice Boltzmann method. This extends our earlier work where the substrates were uniformly hydrophilic or hydrophobic. In steady-state conditions, we calculate the following, as functions of pattern wavelength: (i) the velocity fields of moving bridges, in particular their (time-averaged) terminal velocities; (ii) the deformation of moving bridges, as measured by the deviation of bridge contact angles from their equilibrium values; (iii) the minimum applied force that breaks a moving bridge. In addition, we found that a bridge moving between patterned substrates cannot be mapped onto a bridge moving between uniform substrates endowed with some effective contact angle, even in the limit of very small pattern wavelength compared to bridge width.

1. Introduction

Liquid bridges, also called capillary bridges, or sometimes liquid plugs, are walls or columns of liquid spanning the gap between two bodies, which may be solid surfaces, particles, or other liquids. They occur in many different contexts in nature (the closing of airways in lungs [1], the wet adhesion of insects and tree frogs [2] the feeding of shore birds [3], the spontaneous filling of porous materials [4]), technology (atomic-force microscopy in high-humidity environments [5], soldering [6], weakly-adhesive solid surfaces [7], contact-angle measurements [8]), and even sand art [9]. The study of equilibrium bridges goes back at least to Lagrange: how to find the minimal-area surface enclosing a given volume of liquid, subject to given contact angles as boundary conditions at the surfaces connected by the bridge, plus possibly gravity as a body force.

The problem of a moving bridge has been addressed by a number of authors, but many assume that the liquid completely wets the substrates [10–15]. Other studies have concentrated on particular choices of liquid and substrate, looking experimentally at the effects of gap width, temperature, driving pressure and bridge length on the dynamic contact angle [16,17] or bridge break-up [18]. In addition, several authors have sought to extract the microscopic and apparent contact angles of particle-based models of bridges sliding between smooth [19] or rough [20] substrates, from molecular dynamics or dissipative particle dynamics simulations, respectively,

In earlier work [21] we simulated the motion of a single vertical, 2D liquid bridge spanning the gap between two flat, uniform horizontal solid substrates of given wettabilities, using a multicomponent pseudopotential lattice-Boltzmann method [22,23]. For steady-state bridges moving between identical substrates, we found that, as intuitively expected, hydrophobic bridges experience less drag (at most about 20%) than hydrophilic bridges of the same volume, due to the smaller contact area of the former with the substrates. Furthermore, for slow-moving bridges, contact angles deviate from their equilibrium values by amounts that are proportional to the capillary number, being positive on the advancing side and negative on the receding side but with a complex dependence on the equilibrium contact angles. Finally, we found that the most stable bridges (i.e., those for which breakup is deferred to larger capillary numbers) appear to be those with equilibrium contact angles around 90° under weak gravity.

Here we extend our work of [21] to the case where the substrates are patterned, To our knowledge this has not beet attempted, but is now technologically feasible, and may be relevant in some biological contexts [24].

This paper is organized as follows: in Section 2 we describe our general method for simulating a two-phase flow between patterned substrates. Our results are presented in Section 3: first for the velocity profile and average terminal capillary number of a moving bridge (3.1); then for the average contact angles at the substrates (3.2); finally, we

* Corresponding author at: Centro de Física Teórica e Computacional, Faculdade de Ciências, Universidade de Lisboa, P-1749-016 Lisboa, Portugal.
E-mail address: piteixeira@fc.ul.pt (P.I.C. Teixeira).

https://doi.org/10.1016/j.physd.2024.134322
Received 12 April 2024; Received in revised form 16 July 2024; Accepted 9 August 2024
Available online 12 August 2024

investigate the stability of many types of bridges (i.e., the minimum velocities needed to mobilize or to break them) (3.3). We conclude in Section 4.

2. Method

We perform simulations of liquid bridges using a numerical model based on the same multicomponent pseudopotential lattice-Boltzmann method [22,23] as in our earlier paper [21], where it is described in more detail. The liquid bridges consist of fluid component A and flow between two parallel plates a distance L_y apart; they are surrounded by fluid component B, with a lower density than A. Each component is modelled by a separate set of distribution functions $f_i^{(\sigma)}$, where σ denotes one of the components (A or B) and $\bar{\sigma}$ the other component. Each set of distribution functions describes the local density of each component. The distributions evolve according to the Boltzmann–BGK equation:

$$f_i^{(\sigma)}(\mathbf{x}+\mathbf{c}_i\Delta t, t+\Delta t) - f_i^{(\sigma)}(\mathbf{x},t) = -\frac{\Delta t}{\tau^{(\sigma)}}\left[f_i^{(\sigma)}(\mathbf{x},t) - f_i^{eq(\sigma)}(\mathbf{x},t)\right] + S_i^{(\sigma)}(\mathbf{x},t)\Delta t, \tag{1}$$

where $\mathbf{c}_i$ is the ith velocity vector of the D3Q19 lattice, $\tau^{(\sigma)}$ is the relaxation time, which sets the kinematic viscosity $\nu^{(\sigma)} = (\tau^{(\sigma)} - 1/2)/3$ and Δt is the time step. S_i is the forcing term, which is used to implement the external force that drives the fluid and the internal forces that result in component segregation. As in our earlier paper [21], we set $\tau^{(\sigma)} = 1.2$ for both components: a choice of $\tau^{(\sigma)}$ close to unity is required for stability of the lattice-Boltzmann method [23], and it also ensures that the simulated flow is laminar. A more generic 3D lattice is used, but we set $L_z = 1$ with periodic boundary conditions in the z-direction, which is equivalent to simulating a 2D system. The equilibrium distribution function writes [23,25]:

$$f_i^{eq(\sigma)} = \rho^{(\sigma)} w_i \left[1 + \frac{\mathbf{c}_i\cdot\mathbf{u}^{eq}}{c_s^2} + \frac{(\mathbf{c}_i\cdot\mathbf{u}^{eq})^2}{2c_s^4} - \frac{(\mathbf{u}^{eq})^2}{2c_s^2}\right], \tag{2}$$

where w_i are the discrete weights of the D3Q19 lattice ($w_0 = 1/3$ for $|\mathbf{c}|^2 = 0$, $w_s = 1/18$ for $|\mathbf{c}|^2 = 1$ (short vectors) and $w_l = 1/36$ for $|\mathbf{c}|^2 = 2$) (long vectors), and $c_s = 1/\sqrt{3}$ is the speed of sound in this lattice. $\rho^{(\sigma)}$ stands for the density of component σ. The two fluids interact through a common macroscopic velocity, and via the internal forces. The common macroscopic velocity that is used in the equilibrium distribution function is given by:

$$\mathbf{u}^{eq} = \frac{1}{\rho}\sum_\sigma\left(\sum_i f_i^{(\sigma)}\mathbf{c}_i + \frac{\mathbf{F}^{(\sigma)}\Delta t}{2}\right), \tag{3}$$

where $\rho = \sum_\sigma \rho^{(\sigma)}$ is the total density of the fluid. The total force $\mathbf{F}^{(\sigma)}$ acting on each fluid component is a sum of the external force applied to the fluid (e.g., gravity) and internal forces, which are responsible for fluid segregation and cohesion. The external force $\mathbf{F}^{\text{ext}}$ on each component is proportional to the local density: $\mathbf{F}^{\text{ext},(\sigma)} = \rho^{(\sigma)}\mathbf{F}^{\text{ext}}/\rho$. The forces are implemented using the Guo forcing scheme [26]:

$$S_i^{(\sigma)} = w_i\left(1 - \frac{\Delta t}{2\tau^{(\sigma)}}\right) \times \left[\frac{\mathbf{c}_i}{c_s^2}\left(1 + \frac{\mathbf{c}_i\cdot\mathbf{u}^{eq}}{c_s^2}\right) - \frac{\mathbf{u}^{eq}}{c_s^2}\right]\cdot\mathbf{F}^{(\sigma)}. \tag{4}$$

In this paper, dimensional quantities are given in lattice units, in which the total density ρ, the time step Δt and the lattice spacing Δx are all set to unity.

Segregation between the two components is driven by a local pseudopotential that is a function of the local density of each component. The inter-component force reads:

$$\mathbf{F}^{\text{inter},(\sigma)}(\mathbf{x}) = -\rho^{(\sigma)}(\mathbf{x})\, G_{\sigma\bar{\sigma}} \sum_i w_i\, \rho^{(\bar{\sigma})}(\mathbf{x}+\mathbf{c}_i\Delta t)\,\mathbf{c}_i\,\Delta t, \tag{5}$$

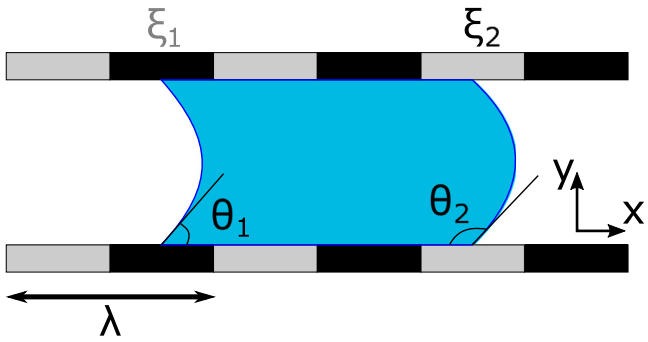

Fig. 1. Schematic of the liquid bridge between patterned substrates. λ is the pattern wavelength and the patterns on the top and bottom substrates are in register.

where $G_{\sigma\bar{\sigma}}$ controls the force magnitude and must be above a certain threshold in order to effect segregation. We set $G_{\sigma\bar{\sigma}} = G_{\bar{\sigma}\sigma} \equiv G_{AB} = 1.3$ in our simulation, where the positive sign implies a repulsive force. The values of the parameters used here follow our previous work [21] and were chosen to yield component segregation and a density difference between the two components. Note that the pseudopotential is simply given by the density in Eq. (5). In addition, there is an intra-component cohesive force acting only on component A:

$$\mathbf{F}^{\text{intra},(A)}(\mathbf{x}) = -\psi^{(A)}(\mathbf{x})\, G_{AA} \sum_i w_i\, \psi^{(A)}(\mathbf{x}+\mathbf{c}_i\Delta t)\,\mathbf{c}_i\,\Delta t, \tag{6}$$

where G_{AA} is the magnitude of the intra-component force, which we set to $G_{AA} = -2$. The minus sign implies an attractive force, which is used to achieve $\rho^{(A)} > \rho^{(B)}$. The pseudopotential in Eq. (6) is $\psi^{(A)} = \rho_0[1 - \exp(-\rho^{(A)}/\rho_0)]$, where we choose the reference density to be $\rho_0 = 1.5$. The resulting equation of state is

$$p = c_s^2\rho^{(A)} + c_s^2\rho^{(B)} + G_{AB}c_s^2\Delta t^2\rho^{(A)}\rho^{(B)} + \frac{1}{2}G_{AA}c_s^2\Delta t^2\psi^{(A)}\psi^{(A)}, \tag{7}$$

where p is the pressure.

The wetting boundary condition is implemented as follows. A field $\phi(\mathbf{x})$ is set to one at the solid nodes and zero at the fluid nodes. This scheme consists in setting a virtual solid density at the solid nodes that controls the contact angle. This density is calculated using a weighted average of the density of the fluid neighbours:

$$\tilde{\rho}^{(\sigma)}(\mathbf{x}) = \chi^{(\sigma)}\frac{\sum_i w_i\rho^{(\sigma)}(\mathbf{x}+\mathbf{c}_i\Delta t)(1-\phi(\mathbf{x}+\mathbf{c}_i\Delta t))}{\sum_i w_i(1-\phi(\mathbf{x}+\mathbf{c}_i\Delta t))}. \tag{8}$$

Parameter χ is different for each component: $\chi^{(A)} = 1 - \xi$ and $\chi^{(B)} = 1 + \xi$, where ξ is the wetting parameter that is used to control the contact angle. If $\xi < 0$, the substrate attracts component A and repels B, whereas if $\xi > 0$, the substrate attracts component B and repels A. We shall refer to these two situations as 'hydrophilic' and 'hydrophobic', respectively. The patterned substrates we simulate consist of a set of alternating regions ('stripes') of length $\lambda/2$ each, where ξ takes the values $\xi_1 < 0$ and $\xi_2 > 0$, as illustrated in Fig. 1. The weights and velocity vectors are those of the D3Q19 lattice. The adhesion force is accounted for in Eqs. (5) and (6) where the sums extend over the solid nodes. The no-slip boundary condition applies to the fluid at the solid nodes, which is implemented using the half-way bounce-back conditions [23].

3. Results

In order to make our results generic, we non-dimensionalize the bridge velocity and the external force applied to the bridge. First, because in our simulations the surface tension γ is constant, we use the capillary number Ca, defined as

$$\text{Ca} = \frac{\langle\rho\rangle\langle u\rangle\nu}{\gamma}, \tag{9}$$

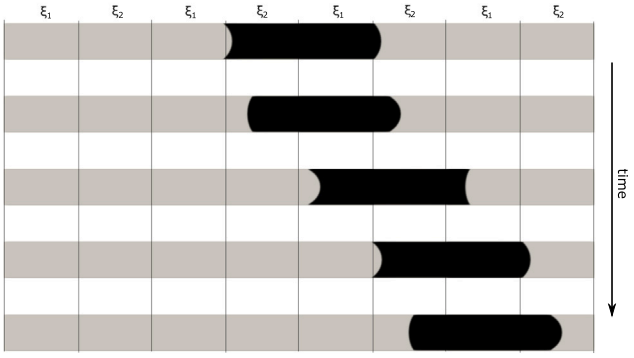

Fig. 2. Snapshots of the liquid bridge moving between patterned substrate with $\lambda = L_x/4$. The vertical lines mark the boundaries between stripes with different ξ's: there is one pair of such stripes per wavelength λ.

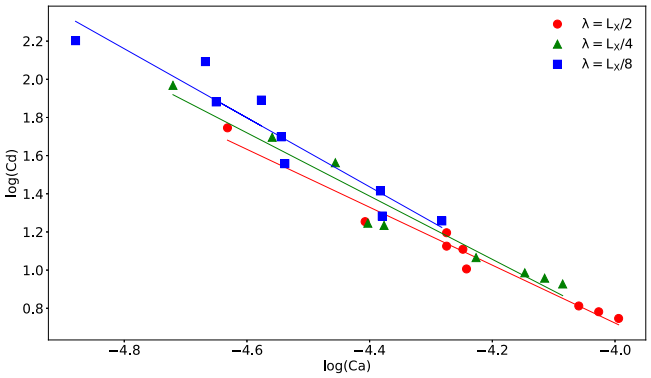

Fig. 3. Logarithm of drag coefficient Cd *vs* logarithm of terminal capillary number of bridge Ca, for pattern wavelengths $\lambda = L_x/2$, $L_x/4$ and $L_x/8$. The lines are linear fits with the following slopes: $n = -1.52 \pm 0.10$ for $\lambda = L_x/2$, $n = -1.66 \pm 0.14$ for $\lambda = L_x/4$, $n = -1.809473 \pm 0.221034$ for $\lambda = L_x/8$.

as a measure of the bridge velocity. Here $\langle\rho\rangle$ is the average density in the simulation domain, and $\langle u\rangle$ is the average velocity of the fluid in space and in time for an integer number of periods in the x-direction. Physically, Ca is a measure of the relative weights of the viscous and surface tension forces. Next, by analogy with our earlier work [21], we define a 'drag coefficient' as:

$$\mathrm{Cd} = \frac{F^{\mathrm{ext}}}{\langle\rho\rangle\langle u\rangle^2 L_x}, \tag{10}$$

where F^{ext} is the applied external force in the fluid, equal to the body force density f_{ext} times the area $L_x \times L_y$. As in our earlier work [21], this body force mimics a pressure gradient driving the motion of the bridge. In steady-state motion, for which the average resultant force on the bridge must vanish, this is a measure of the averaged drag, or frictional, force exerted by the substrates on the liquid, or equivalently by the liquid on the substrates.

In the simulations, we initialize the densities of the two components as follows: inside the liquid bridge $\rho^{(A)} = 4$ and $\rho^{(B)} = 0.001$, and outside $\rho^{(A)} = 0.001$ and $\rho^{(B)} = 2$; the density difference is thus $\Delta\rho \approx 2$. We chose $\xi_1 = -0.8987$ and $\xi_2 = 0.7635$, which give contact angles of 50° and 130° (symmetric around 90°) at the hydrophilic and hydrophobic stripes, respectively. Except where stated otherwise, the simulation box dimensions are $L_x \times L_Y = 1024 \times 64$ and the two initially flat interfaces which bound the liquid bridges are placed at $x_1 = 3L_x/8$ and $x_2 = 5L_x/8$. Using the Laplace test, we obtain for the surface tension between the two fluids with the internal forces described in the previous section $\gamma = 0.342 \pm 0.001$. An external force is then applied in the direction x parallel to the substrates. After an initial transient, whose duration depends on the contact angles and the magnitude of the applied force, a steady-state is established in which the bridge attains a terminal velocity. As the bridge moves across the alternating hydrophilic and hydrophobic stripes, its interfaces periodically change shape, as illustrated in Fig. 2, This motion is intrinsically non-steady, as the flow field is constantly being reconfigured in the vicinity of the interfaces, as can be seen in the video (see Supplementary Material). However the flow inside and outside the bridge is mostly Poiseuille, as the interfaces are set far enough apart that they do not interact with each other. This occurs because the two fluids are immiscible, and therefore there is no relative velocity in the direction normal to the interfaces of the liquid bridge. In what follows, we shall refer to this flow as 'steady state' if it is periodic. It would be of interest to study the limit of a very thin liquid bridge, or film, but this would be non-trivial using the lattice Boltzmann method, as the discreteness of the lattice might introduce numerical artefacts.

In the remainder of this section we present results for the terminal velocity, the contact angles of the bridge at the substrates, and the maximum force a bridge can withstand without breaking. One question that naturally arises is: can we map the results for a bridge moving between patterned substrates onto those for a bridge moving between uniform substrates (our earlier work [21]) characterized by some effective contact angle (equivalently, effective ξ)? Naively one might expect this to be the case when the bridge is much wider than the pattern wavelength, so the interfaces fluctuate very rapidly around some mean shape. However, the answer appears to be 'no': we were unable to find a single effective ξ that, for a given external force, would reproduce both the terminal velocity and the mean contact angles of a bridge moving between patterned substrates.

3.1. Average terminal capillary number

Fig. 3 shows the dependence of the terminal capillary number of a liquid bridge on the drag coefficient, for pattern wavelengths $\lambda = L_x/2$. $L_x/4$ and $L_x/8$. It is seen that Ca $\sim$ Cd^{-n} with an exponent $0 < n < 1$ that depends on the patterns wavelength. For a bridge moving between homogeneous substrates, it follows from dimensional analysis that $n = 1$, with a proportionality constant that is a decreasing function of ξ, i.e., it is smaller for hydrophobic substrates than for hydrophilic ones [21]. The fits to the data in Fig. 3 show that n is an increasing function of λ, i.e., they are consistent with $n \to 1$ in the uniform-substrate ($\lambda \to \infty$) limit. For patterned substrates, $n \neq 1$ because the system is non-steady, while the calculations in Ref. [21] assumed a steady state. There are periodic accelerations whenever the interfaces change shape that perturb this assumption. This is why n deviates more from unity for smaller λ. Moreover, n is less than one because the bridge's velocity for the same external force tends to decrease as λ decreases.

Here it would have been physically more transparent to plot Ca *vs* Cd Ca Re (with Re $= L_x u/\nu$ a Reynolds number), which is a measure of external force relative to capillary force. However, we found the result is too noisy to be informative. We do plot this quantity in the inset of Fig. 6, for which the data are less noisy.

3.2. Average contact angle

As mentioned before, the bridge interfaces periodically change shape as they pass over the boundaries between hydrophilic and hydrophobic regions. In Fig. 4 we plot the maximum and minimum values of the bridge advancing contact angles, as well as their average values. The averages are calculated in time and for an integer number of periods. The maximum and minimum angles for each Ca are about 10° larger than the equilibrium angles for each ξ, which is a consequence of the bridge motion (the advancing angle is an increasing function of the bridge velocity). The average, maximum and minimum angles are fairly independent of Ca, at least for this range of parameters. This suggests that the bridge interfaces have enough time to relax to something

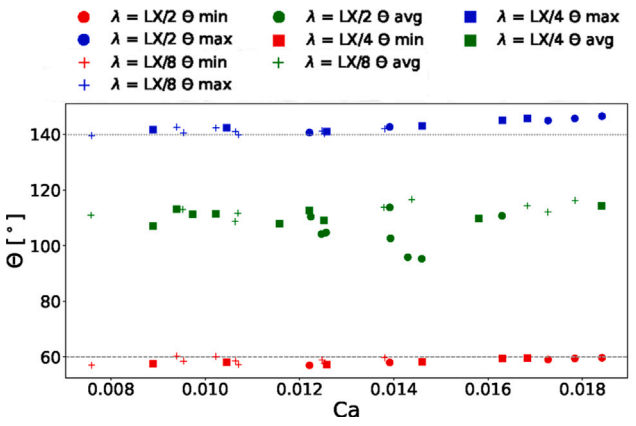

Fig. 4. Maximum (blue symbols), minimum (red symbols) and mean (green symbols) contact angles on advancing side of bridge *vs* terminal capillary number Ca for three different values of λ. The dashed lines are a guide for the eye to illustrate the small increase of the angles with Ca.

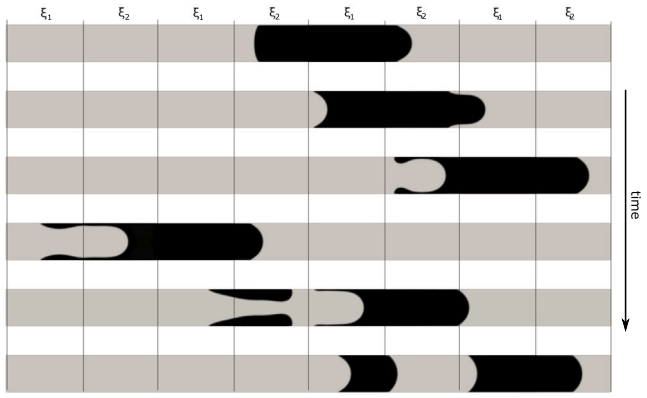

Fig. 5. Snapshots of the liquid bridge breaking up for a patterned substrate with wavelength $\lambda = L_x/4$.

like their equilibrium shapes. The maximum contact angle, however, exhibits a slight increase for the larger Ca. For uniform substrates [21], the advancing angle increases by ∼5° when Ca is increased by the same amount as here, which is compatible with our observations for patterned substrates. However, this difference is small when compared to the fluctuations in the angle values (which are not steady), and therefore difficult to detect. Furthermore, we cannot go to much larger Ca because the bridge will break, as will be discussed later.

3.3. Breaking bridges

If the external force (or, equivalently, the terminal velocity) is too small the bridge will not move as it gets pinned at the stripe boundaries, where ξ is discontinuous. On the other hand, if it is too large the bridge will break. This is qualitatively different from the uniform (unpatterned) substrates case, for which an infinitesimally small external force is enough to set the bridge in motion. The patterning thus appears to endow the substrates with an effective static friction. A similar effect occurs in the flow of foam through non-uniform cross-section channels [27]. Interestingly, the minimum external force that is needed to mobilize a bridge appears to be independent of pattern wavelength, a curious (and likely coincidental) analogy with the Coulomb friction of solids.

Fig. 5 illustrates the breaking-up process of a liquid bridge. First, its contact line gets pinned at the boundary between stripes and undergoes a fingering instability. Then the bridge starts growing two tails at the substrates, which later break off the bridge and coalesce to form a separate liquid bridge, trailing the original one.

In contrast, the maximum capillary number (velocity) for which the bridge does not break, Ca_{max}, does depend on the pattern wavelength, as shown in Fig. 6. As λ increases, the substrates become more and more uniform-like and Ca_{max} is expected to saturate. It does so at ∼0.02. For comparison, this is approximately equal to Ca_{max} for uniform substrates with $\xi = 0.6$, corresponding to a contact angle of about 120° while the bridge was most stable for $\xi = -0.6$ (65°) [21]. We further note that, for the same external force F^{ext}, the bridge between patterned substrates moves more slowly than the bridge between uniform substrates, because the former slows down when crossing boundaries between stripes, at which, as we saw above, it changes shape and the flow profiles both inside and outside it are reconfigured. One would then expect Ca_{max} to decrease as $\lambda \to 0$, and more and more stripe boundaries need to be crossed, as indeed happens.

Finally, we also explored a 3D liquid bridge in a tube with circular cross section of the same diameter as L_y in the 2D case, and an axisymmetric stripe pattern (equivalent to rolling up the 2D system around the x-axis). Preliminary results indicate that the force needed to break up the liquid bridge in this geometry is larger by a factor of almost 2 than that for the 2D bridge. We speculate that this may be due to the larger contact area between bridge and substrate. This work is in progress. Snapshots of the breaking-up process are depicted in Fig. 7, which resembles the process in 2D.

4. Conclusions

We addressed the motion of 2D liquid bridges between periodically-patterned substrates, consisting of alternating hydrophilic and hydrophobic stripes all of the same length. One important conclusion is that in general, this system cannot be mapped onto a 2D liquid bridge moving between uniform substrates of some effective wettability. Moreover, whether the transition between stripes is discontinuous or continuous does not affect our results significantly.

As the bridge transitions from one stripe to the next, the shapes of its interface change periodically, to accommodate the varying boundary conditions, and the flow pattern near the interfaces, both inside and outside the bridge, is reconfigured, but elsewhere it remains roughly Poiseuille. After an initial transient, the bridge subjected to a constant external driving force attains a steady state characterized by a well-defined average terminal velocity. Suitably non-dimensionalized, this average terminal velocity has an inverse power-law dependence on the also non-dimensionalized external force, with an exponent $0 < n < 1$ which is an increasing function of the pattern wavelength. In contrast, the contact angles at the substrates also fluctuate, but appear not to depend (or depend only very weakly) on the pattern wavelength. Unlike for uniform substrates, a finite external force is required to set the bridge in motion, which – at least in the ranges of parameters investigated – is independent of pattern wavelength. On the other hand, the maximum velocity for which the bridge will not break (alternatively, the minimum velocity needed to break the bridge) is an increasing function of pattern wavelength that saturates as the uniform-substrate limit is approached.

Possible extensions of our work include the study of a 3D bridge moving through an axially-striped cylindrical tube, which was only illustrated here. Although the bridge behaves in qualitatively the same way as in 2D, some quantitative differences have emerged. Another possibility is to simulate other striped patterns, e.g., longitudinal, which would break the axial symmetry and make the system more truly 3D. An extension to non-Newtonian fluid bridges would also be interesting.

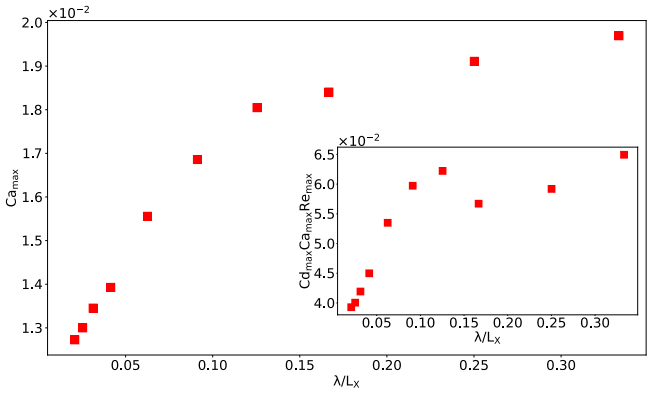

Fig. 6. Maximum capillary number Ca_{max} (proportional to the velocity) for which the liquid bridge does not break *vs* pattern wavelength λ. The inset depicts $Cd_{max}Ca_{max}Re_{max}$, which is a measure of the external force, *vs* pattern wavelength λ, where Cd_{max} and $Re_{max} = \langle u \rangle_{max} L_y/\nu$ are the maximum drag coefficient and Reynolds number for which the liquid bridge does not break.

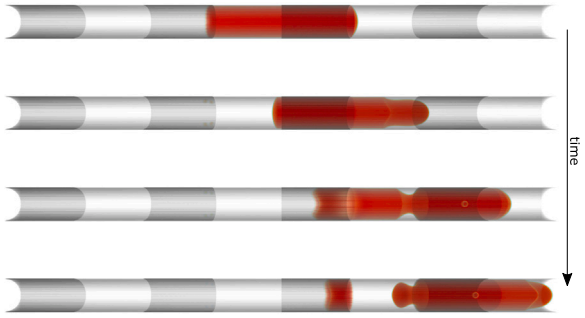

Fig. 7. Break-up of an axisymmetric bridge moving through a striped tube.

CRediT authorship contribution statement

Margarida S. Rodrigues: Visualization, Investigation, Data curation. **Rodrigo C.V. Coelho:** Writing – original draft, Visualization, Supervision, Software, Resources, Methodology, Investigation, Funding acquisition, Conceptualization. **Paulo I.C. Teixeira:** Writing – original draft, Supervision, Project administration, Funding acquisition, Conceptualization.

Declaration of competing interest

The authors declare the following financial interests/personal relationships which may be considered as potential competing interests: Rodrigo C. V. Coelho reports financial support was provided by Foundation for Science and Technology. Paulo I. C. Teixeira reports financial support was provided by Polytechnic Institute of Lisbon. Margarida S. Rodrigues reports financial support was provided by Polytechnic Institute of Lisbon. Paulo I. C. Teixeira reports financial support was provided by Foundation for Science and Technology. Margarida S. Rodrigues reports financial support was provided by Foundation for Science and Technology. Rodrigo C. V. Coelho reports financial support was provided by Polytechnic Institute of Lisbon. If there are other authors, they declare that they have no known competing financial interests or personal relationships that could have appeared to influence the work reported in this paper.

Data availability

Data will be made available on request.

Acknowledgements

We acknowledge financial support from the Portuguese Foundation for Science and Technology (FCT), Portugal under the contracts: EXPL/FIS-MAC/0406/2021 (DOI: 10.54499/EXPL/FIS-MAC/0406/2021), PTDC/FIS-MAC/5689/2020 (DOI: 10.54499/PTDC/FIS-MAC/5689/2020), UIDB/00618/2020 (DOI: 10.54499/UIDB/00618/2020) and UIDP/00618/2020 (DOI: 10.54499/UIDP/00618/2020), and from the Polytechnic Institute of Lisbon, Portugal through project IPL/IDI&CA2023/LIQBRIDGE_ISEL. This work was produced with the support of UC-LCA and it was funded by FCT I.P, Portugal. under the project Advanced Computing Project 2023.10412.CPCA.A2, platform Navigator.

Appendix A. Supplementary data

Supplementary material related to this article can be found online at https://doi.org/10.1016/j.physd.2024.134322.

References

[1] A.M. Alencar, A. Majumdar, Z. Hantos, S.V. Buldyrev, H.E. Stanley, B. Suki, Crackles and instabilities during lung inflation, Phys. A 357 (2005) 18–26.
[2] B.N.J. Persson, Wet adhesion with application to tree frog adhesive toe pads and tires, J. Phys.: Condens. Matter. 19 (2007) 376110.
[3] M. Prakash, D. Queré, J.W.M. Bush, Surface tension transport of prey by feeding shorebirds: The capillary ratchet, Science 320 (2008) 931–934.
[4] E.W. Washburn, The dynamics of capillary flow, Phys. Rev. 17 (1921) 273–283.
[5] Y. Men, X. Zhang, W. Wang, Capillary liquid bridges in atomic force microscopy (AFM): Formation, rupture, and hysteresis, J. Chem. Phys. 131 (2009) 184702.
[6] R.B. Edwards, Joint tolerances in capillary copper piping joints, Weld. J. 6 (1972) 321–324.
[7] L. Vagharchakian, F. Restagno, L. Léger, Capillary bridge formation and breakage: a test to characterize antiadhesive surfaces, J. Phys. Chem. B 113 (2009) 3769–3775.
[8] N. Nagy, Contact angle determination on hydrophilic and superhydrophilic surfaces by using $r-\theta$-type capillary bridges, Langmuir 35 (2019) 5202–5212.
[9] M. Pakpour, M. Habib, P. Møller, D. Bonn, How to construct the perfect sandcastle, Sci. Rep. 2 (2012) 545.
[10] P.D. Howell, S.L. Waters, J.B. Grotberg, The propagation of a liquid bolus along a liquid-lined flexible tube, J. Fluid Mech. 406 (2000) 309–335.
[11] D.M. Campana, S. Ubal, M.D. Giavedoni, F.A. Saita, Stability of the steady motion of a liquid plug in a capillary tube, Ind. Eng. Chem. Res. 45 (2007) 1803–1809.
[12] S. Ubal, D.M. Campana, M.D. Giavedoni, F.A. Saita, Stability of the steady-state displacement of a liquid plug driven by a constant pressure difference along a prewetted capillary tube, Ind. Eng. Chem. Res. 47 (2008) 6307–6316.
[13] J.C. Magniez, M. Baudoin, C. Liu, F. Zoueshtiagh, Dynamics of liquid plugs in prewetted capillary tubes: from acceleration and rupture to deceleration and airway obstruction, Soft Matter 12 (2016) 8710–8717.
[14] H. Fujioka, D. Halpern, J. Ryans, D.P. Gaver III, Reduced-dimension model of liquid plug propagation in tubes, Phys. Rev. Fluids 1 (2016) 053201.
[15] P. Favreau, A. Duchesne, F. Zoueshtiagh, M. Baudoin, Motion of long levitating drops in tubes in an anti-bretherton configuration, Phys. Rev. Lett. 125 (2020) 194501.
[16] Y.D. Ma, Motion effect on the dynamic contact angles in a capillary tube, Microfluid. Nanofluid. 12 (2012) 671–675.
[17] V. Srinivasan, S. Khandekar, N. Bouamrane, F. Lefevre, J. Bonjour, Motion of an isolated liquid plug inside a capillary tube: effect of contact angle hysteresis, Exp. Fluids 56 (2015) 14.
[18] Y. Kazoe, T. Matsuno, I. Yamashiro, K. Mawatari, T. Kitamori, Control of liquid plug motion in microchannels, Lab Chip 18 (2018) 1234–1246.
[19] J.C. Fernandez-Toledano, T.D. Blake, J. De Coninck, Taking a closer look: A molecular-dynamics investigation of microscopic and apparent dynamic contact angles, J. Colloid Interface Sci. 587 (2021) 311–323.
[20] E. Lee, F. Müller-Plathe, Contact line friction and dynamic contact angles of a capillary bridge between superhydrophobic nanostructured surfaces, J . Chem. Phys. 157 (2022) 024701.
[21] R.C.V. Coelho, L.A.R.G. Cordeiro, R.B. Gazola, P.I.C. Teixeira, Dynamics of two-dimensional liquid bridges, J. Phys.: Condens. Matter. 34 (20) (2022) 205001.
[22] X. Shan, H. Chen, Lattice Boltzmann model for simulating flows with multiple phases and components, Phys. Rev. E 47 (1993) 1815–1819.

[23] T. Krüger, H. Kusumaatmaja, A. Kuzmin, O. Shardt, G. Silva, E.M. Viggen, The Lattice Boltzmann Method - Principles and Practice, Springer International Publishing, ISBN: 978-3-319-44647-9, 2016.

[24] J. Chi, X. Zhang, Y. Wang, C. Shao, S. L., Y. Zhao, Bio-inspired wettability patterns for biomedical applications, Mater. Horiz. 8 (2021) 124–144.

[25] R.C.V. Coelho, A. Ilha, M.M. Doria, R.M. Pereira, V.Y. Aibe, Lattice Boltzmann method for bosons and fermions and the fourth-order Hermite polynomial expansion, Phys. Rev. E 89 (2014) 043302.

[26] Z. Guo, C. Zheng, B. Shi, Discrete lattice effects on the forcing term in the lattice Boltzmann method, Phys. Rev. E 65 (2002) 046308.

[27] W.R. Rossen, Theory of mobilization pressure gradient of flowing foams in porous media: I. Incompressible foam, J. Colloid Interface Sci. 136 (1990) 1–16.